A&A 435, 587–594 (2005)
DOI: 10.1051/0004-6361:20042256

Astronomy & Astrophysics

CO_2 synthesis in solid CO by Lyman-α photons and 200 keV protons

M. J. Loeffler[1,2], G. A. Baratta[1], M. E. Palumbo[1], G. Strazzulla[1], and R. A. Baragiola[2]

[1] INAF-Osservatorio Astrofisico di Catania, via Santa Sofia 78, 95123 Catania, Italy
e-mail: mepalumbo@ct.astro.it
[2] University of Virginia, Laboratory for Atomic and Surface Physics, Thornton Hall, Charlottesville, VA 22903, USA

Received 26 October 2004 / Accepted 25 January 2005

Abstract. We have studied the synthesis of carbon dioxide from solid carbon monoxide at 16 K induced by photolysis with Lyman-α photons and by irradiation with 200 keV protons to quantitatively compare the effects of photolysis and ion irradiation on CO ice and to determine the importance of these processes in interstellar ice grains. The CO and CO_2 concentrations during irradiation of an initially pure CO film evolve with fluence to a saturation value, a behaviour that is explained by a two-state model. Our results indicate that the initial CO_2 production rates for both radiation processes are similar when normalized to the absorbed energy and that the solid CO_2 abundance observed in the interstellar ices cannot be explained only by radiolysis and photolysis of pure solid CO.

Key words. astrochemistry – molecular processes – methods: laboratory – techniques: spectroscopic – ISM: molecules – infrared: ISM

1. Introduction

A central problem in astrophysics is molecular synthesis on interstellar grains. The carbon dioxide molecule, difficult to observe from the ground because its main infrared vibrational bands are obscured by the Earth's atmosphere, was first detected in the interstellar medium by d'Hendecourt & Jourdain de Muizon (1989) through its weaker 15.2 μm band in IRAS (Infrared Astronomical Satellite) low resolution spectra. This discovery confirmed expectations based on the abundance of a possible precursor molecule, CO, and on the presence of CO_2 in comets that are thought to result from accretion of interstellar grains. The Infrared Space Observatory (ISO), free from atmospheric absorption, allowed the observation of interstellar solid CO_2 in many different interstellar environments (e.g., de Graauw et al. 1996; Gerakines et al. 1999), which may provide important clues on how the molecule is formed. Since there is a very small abundance of gas phase CO_2 in the interstellar medium, it is reasonable to expect that the molecule is synthesized on grains. The correlation between CO and CO_2 column densities (Gerakines et al. 1999) suggests that an important CO_2 synthesis mechanism is oxidation of condensed CO. This process may be induced efficiently by O atoms made available from dissociation of adjacent CO, H_2O, O_2, etc., by incoming radiation such as Lyman-α, stellar winds, or cosmic rays. Recently it has been suggested that in dense clouds solid carbon dioxide can be formed after cosmic ray irradiation of carbon grains with a water ice cap (Mennella et al. 2004). The presence of CO_2 in dark clouds could also be due to reactions between gas phase O and a carbon monoxide surface (Roser et al. 2001).

Here we address the radiation pathways, comparing the efficiency of CO_2 synthesis from pure carbon monoxide ice by 200 keV protons and Lyman-α (10.2 eV) photons. This topic has been researched recently by Gerakines & Moore (2001), who reported that Lyman-α is 3.5 times more efficient than 800 keV protons in synthesizing CO_2 on virgin CO per unit incident energy. This is surprising for several reasons. First, the large band-gap of solid CO makes the ionization channel energetically unavailable for Lyman-α photolysis, and previous experiments (Gerakines et al. 1996) gave an extremely small cross section for CO_2 photosynthesis in CO $\sim 10^{-20}$ cm^2. Second, previous studies revealed that erosion yields from water ice by fast protons (Brown et al. 1984) are much larger than by Lyman-α (Westley et al. 1995a) due to a dominant double collision channel only available to ions, which is manifested in a quadratic dependence of the sputtering yield on electronic stopping power (S_e; Baragiola et al. 2003). The erosion of CO is expected to be analogous since in this case the sputtering yield is also proportional to S_e^2 (Brown et al. 1984). We also note that the initial radiation effects on condensed methane and methanol were found to be similar for 10.2 eV photons and 30 keV He^+ ions (Baratta et al. 2002). Furthermore it has been shown that crystalline water ice is converted into amorphous ice by Lyman-α photons with an efficiency comparable to that of fast ions (Leto & Baratta 2003). In view of the apparent discrepancies of results here we examine

the possibility that in previous experiments (Gerakines & Moore 2001) CO_2 molecules desorbed from vacuum system walls and condensed on the sample. To discriminate against those molecules, we used isotopic labelling.

2. Experimental methods

Experiments were performed in a stainless steel vacuum chamber with base pressure of about 10^{-7} mbar with the setup described by Baratta et al. (2002), using a Bruker Equinox 55 FTIR spectrometer at a resolution of 1 cm^{-1}. The CO sample was condensed on a silicon substrate cooled to 16 K, which is transparent to the infrared light in the range of interest, allowing measurements of transmission spectra. The substrate forms an angle of 45° with the infrared beam. A concern in these experiments was that H_2O and CO_2, unavoidably absorbed on the internal surfaces of the vacuum chamber, are photodesorbed by scattered UV photons during the operation of the UV lamp and can condense on the cold sample. This has been confirmed in control experiments: H_2O and CO_2 condensed on a bare Si surface during Lyman-α irradiation. Furthermore, we have accurately verified that when the lamp is turned off, no discernable amount of CO_2 condenses from the residual gas. Condensation of uncontrolled CO_2 and H_2O could significantly alter the derived CO_2 production rates for two main reasons: indistinguishable CO_2 added to the surface and absorption of Lyman-α radiation by water before it reaches the CO ice (reducing the actual photon flux on the CO ice). These problems only slightly affect the results in the case of ion irradiation, because the ion beam only impinges on a surface comparable with the sample dimension. Again we have verified that no CO_2 condenses on the sample when the ion beam is turned off.

For those reasons, we grew the films with isotopically labelled ^{13}CO; irradiated ^{13}CO ice yields $^{13}CO_2$ with a shifted ν_3 infrared absorption band (2281 cm^{-1} vs. 2343 cm^{-1} for adventitious $^{12}CO_2$). The condensation rate of CO, 34 nm min^{-1}, was ~1000 times larger than that of the background gas, mostly water. To prevent reactions with the substrate and minimize contamination of the CO film during the experiments, the sample was grown as an Ar-CO-Ar sandwich (Gerakines et al. 1996), using ~130 nm thick Ar films. All calculations of column density were done by first converting the spectra (I_f) into optical depth units: $-\ln(I_f/I_o)$, where I_o is the spectrum measured before depositing any film. Next, after fitting a straight baseline, we calculated the band area, divided by the band strength A, and corrected for 45° incidence, to obtain the column density of the film. To quantify the optical depth we assumed that the band strengths of ^{13}CO and $^{13}CO_2$ were the same as for ^{12}CO and $^{12}CO_2$, $A = 7.6 \times 10^{-17}$ cm molecule^{-1} ($^{13}CO_2$) and $A = 1.1 \times 10^{-17}$ cm molecule^{-1} (^{13}CO) (Yamada & Person 1964; Jiang et al. 1975). Comparing the column density measured by infrared spectroscopy with the film thickness measured by laser interferometry (Baratta & Palumbo 1998), we derive that the density of the CO film in our experimental conditions is 0.81 g cm^{-3}. Other measurements give a value of 0.80 g cm^{-3} (Roux et al. 1980).

A microwave-discharge hydrogen lamp produced Lyman-α radiation at 10.2 eV, which enters the vacuum chamber through an MgF_2 window[1]. To increase the light flux on the sample, we used a coaxial aluminum cylinder to reflect light onto the sample (Westley et al. 1995a). With this setup, the photon incidence is within a few degrees of the normal to the surface. The amount of UV light produced by the hydrogen lamp is not constant with time, and thus one needs to monitor the discharge constantly. Using the technique described by Westley et al. (1995a) and Baratta et al. (2002), a negatively biased Pt wire was placed in the beam path, and the current produced by electron emission was used to determine the UV flux on the sample. This wire detector was calibrated as described by Baratta et al. (2002) by measuring the production of O_3 from solid O_2 and using published cross section values (Gerakines et al. 2000). The sensitivity of this detector was found to be 5.7×10^{12} photons cm^{-2} s^{-1} nA^{-1}. To be able to quantify photolysis and ion beam radiolysis in units of absorbed energy we require the absorption cross section of 10.2 eV photons by the CO film, which was unknown. We used the two-film method described by Baratta et al. (2002), using 140 nm and 262 nm films, and obtained an absorption cross section $\sigma_a = (2.6 \pm 0.1) \times 10^{-18}$ cm^2 (absorption coefficient $\alpha = 4.3$ μm^{-1}). We have verified that α remains constant in the range of photon fluences considered. This is not always the case as has been discussed by Baratta et al. (2002).

For the ion irradiation experiments we used an electrostatic 200 kV ion implanter (Danfysik) with magnetic mass separation. The ion beams were scanned electrostatically to ensure a uniform fluence on the target. Typical fluxes were 1×10^{12} ions cm^{-2} s^{-1}.

In some experimental setups, normal incidence is used for infrared analysis. It is important to note that at oblique incidence P polarization may show added features for strong transitions that are related to the strong variation of the real part of the refractive index (n) and do not correspond to any peak of the imaginary part (k), that is to say are not directly related to the absorption coefficient α, through the relation $\alpha = 4\pi k/\lambda$ (Baratta & Palumbo 1998). An example is given in Fig. 1, where the strong absorption band of ^{13}CO (2091 cm^{-1}) shows added features with P polarized light, while the weaker $^{13}C^{18}O$ band (2040 cm^{-1}) shows no detectable difference between the two different polarizations. In the case of normal

[1] We need to consider that the discharge lamps are not monochromatic, with a spectrum of the emitted radiation depending on experimental conditions, such as pressure in the discharge tube and gas mixture ratio. For example, the operating conditions adopted by Westley et al. (1995b; see their Fig. 1) produce negligible UV radiation outside the Lyman-α line; on the other hand, the Lyman-α emission accounts for at most 5% of the total lamp intensity in the operating conditions used by Cottin et al. (2003; see their Fig. 1). The operating conditions of the UV lamp adopted in this work are more similar to those used by Westley et al. (1995a,b), and thus we assume that we have a similar spectrum. However we cannot exclude the possibility that lower energy photons are present. Cottin et al. (2003) have estimated that in their experimental conditions the average photon energy is about 7.4 eV. At any rate, this would introduce an uncertainty of at most 30% in G values and energy dose calculations (Sect. 4.2).

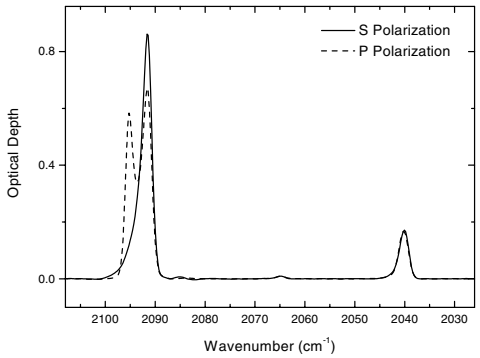

Fig. 1. Comparison of optical absorption depth for S and P polarization, for a 140 nm ^{13}CO film, grown and held at 16 K.

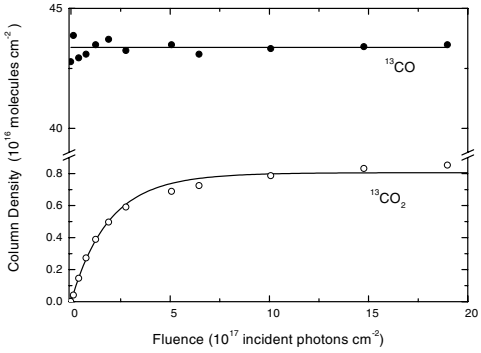

Fig. 2. The column density of ^{13}CO and $^{13}CO_2$ as a function of the incident photon fluence after correcting for reflection at the film surface and absorption by condensed water. The $^{13}CO_2$ production has been modeled using a two component model (−), which is described in the discussion section and given as Eq. (8); no attempt has been made to model the destruction of ^{13}CO by UV photolysis.

incidence, because of symmetry, the spectra are the same at any polarization. All calculations in the following use S polarization, which is more directly comparable with other experiments at normal incidence described in the literature.

3. Results

3.1. UV photolysis

The initial goal was to measure the destruction of ^{13}CO as a function of photon fluence but, as Fig. 2 shows, the change in the main band was too small to detect it outside experimental uncertainties. The same figure shows the column density of $^{13}CO_2$ formed after photolysis. This will be discussed in detail in Sect. 4.1. The amount of carbon dioxide formed requires a reduction of the column density of CO too small to be measured within uncertainties.

Figure 3 shows the infrared absorption in the CO_2 ν_3 region, where the bands of both adventitious $^{12}CO_2$ and $^{13}CO_2$ produced in the film from ^{13}CO can be seen. The larger width of the $^{12}CO_2$ band suggests that the transition has been perturbed by a different environment, like water, consistent with the observation that background water accompanies the deposition of $^{12}CO_2$ during UV photolysis. The narrowness of the $^{13}CO_2$ band indicates that one main transition occurs, without

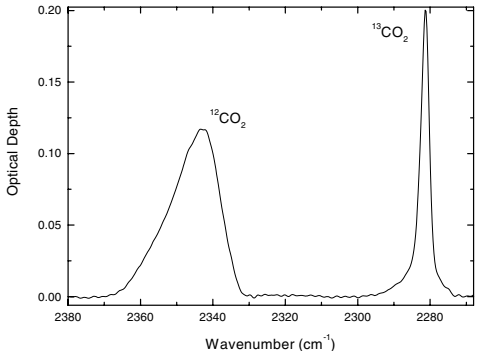

Fig. 3. Optical depth of $^{12}CO_2$ and $^{13}CO_2$ peaks after an incident fluence of 1.89×10^{18} photons cm^{-2} on a 262 nm (4.4×10^{17} molecules cm^{-2}) ^{13}CO film at 16 K.

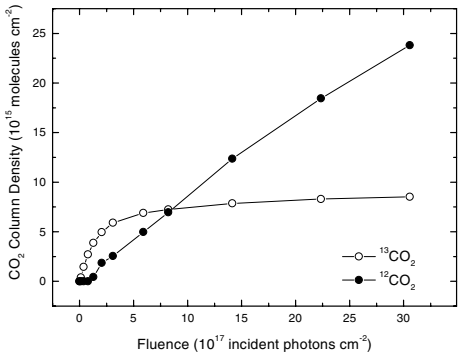

Fig. 4. Production curves of $^{13}CO_2$ and $^{12}CO_2$ during photolysis of a 262 nm ^{13}CO ice film at 16 K. Here no correction has been made for water absorption, because the water is mixed with the $^{12}CO_2$.

any major perturbation, showing the effectiveness of the top Ar layer in shielding the ^{13}CO matrix from contamination.

Figure 4 shows the column density of $^{13}CO_2$ and $^{12}CO_2$ as a function of incident photon fluence, where one can see that the buildup of $^{12}CO_2$ contamination becomes an important factor after long photolysis times. We have verified that the $^{12}CO_2$ growth is linear with photon fluence and stops when the lamp is turned off, indicating that $^{12}CO_2$ is deposited only during the UV photolysis experiments. Comparable buildup of $^{12}CO_2$ contamination was also observed after photolysis of O_2 during the experiments done to calibrate the platinum wire photodetector.

3.2. Ion irradiation

To study the effect of ion irradiation, we used the same experimental conditions as the UV photolysis experiments, except that the incidence angle of the projectiles was 45° instead of normal to the surface. We bombarded ^{13}CO with 200 keV protons with fluences up to 1.73×10^{15} ions cm^{-2}. The column density of ^{13}CO is seen to decrease during ion bombardment (Fig. 5). This decrease cannot be attributed to the removal of material by sputtering. An extrapolated value for the sputtering yield of a surface of CO exposed to vacuum for ~200 keV protons is 10 CO/proton (Brown et al. 1984), which means that about 3% of the material would have been removed at the highest fluence. However, the top Ar layer used in our experiments

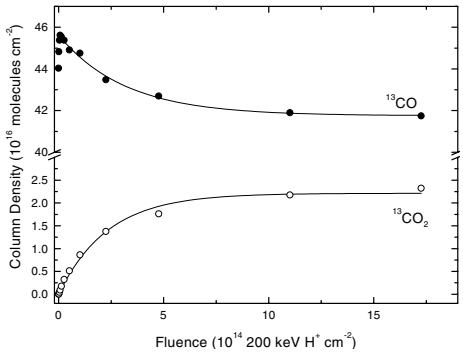

Fig. 5. Variation of column densities of ^{13}CO and $^{13}CO_2$ due to 200 keV H^+ irradiation of a 262 nm ^{13}CO film at 16 K. Both the destruction of ^{13}CO and creation of $^{13}CO_2$ were modeled (–) by the two component model described in the discussion section.

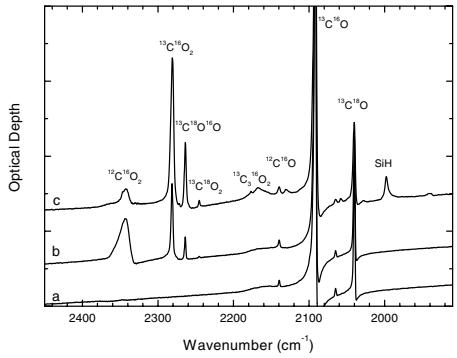

Fig. 6. Infrared spectra at 16 K, before **a)**, after **b)** irradiation with 2×10^{18} photons cm^{-2}, and after **c)** irradiation with 1.73×10^{15} 200 keV H^+ cm^{-2} of a 262 nm ^{13}CO film. In the case of ion irradiation the feature labelled SiH is due to implantation of H ions in the silicon substrate which form Si-H bonds.

would impede most of the energized CO from escaping and a smaller fraction of CO would be injected into the Ar film but still be detectable in the spectra at essentially the same infrared frequency. Thus the decrease of the column density of solid CO has to be attributed to the formation of other chemical species, mainly carbon dioxide and more refractory suboxides (Strazzulla et al. 1997; Gerakines & Moore 2001). The asymptotic value is reached when the amount of CO destroyed equals the amount re-formed (e.g., by CO_2 destruction).

After both ion irradiation and UV photolysis, carbon dioxide is the most abundant species formed, however several new absorption features appear in the 2400–1900 cm^{-1} spectral range shown in Fig. 6 and listed in Table 1. It has been shown that after ion irradiation and UV photolysis of ^{12}CO ice, carbon-chain oxides are formed (e.g., Strazzulla et al. 1997; Gerakines & Moore 2001; Trottier & Brooks 2004). We believe that carbon oxides are in fact responsible for most of the features listed in Table 1. However, due to isotopic labelling, the comparison with published data is not straightforward. In Table 1 we suggest a tentative identification of the ^{13}C-chain oxides based on the identification given by Trottier & Brooks (2004) and assuming that peak position scales as the inverse of the square root of the reduced mass.

All spectra in Fig. 6 show a "dip" at about 2087 cm^{-1} close to the strong $^{13}C^{16}O$ absorption band. This is due to the sharp variation of the real part of the refractive index (n) of CO ice at this wavenumber and also depends on the optical properties of the substrate. A similar feature is present at about 2038 cm^{-1} close to the $^{13}C^{18}O$ absorption band. In the case of ion irradiation the feature labelled SiH is due to implantation of H ions in the silicon substrate which form Si-H bonds.

Table 1. Peak position of the bands observed after ion irradiation and UV photolysis of ^{13}CO ice and their identification.

Peak position (cm^{-1})	Molecule
2343	$^{12}C^{16}O_2$
2281	$^{13}C^{16}O_2$
2263	$^{13}C^{18}O^{16}O$
2246	$^{13}C^{18}O_2$
2176	$^{13}C_3\,^{16}O_2$
2166	$^{13}C_5\,^{16}O_2$
2140	$^{12}C^{16}O$
2130	$^{13}C_7\,^{16}O_2$
2091	$^{13}C^{16}O$
2065	$^{13}C^{17}O$
2057	$^{13}C_7\,^{16}O_2$
2040	$^{13}C^{18}O$
2029	$^{13}C_5\,^{16}O_2$
1940	$^{13}C_2\,^{16}O$

4. Discussion

4.1. Fit of experimental data

The radiolysis of gaseous CO was reviewed by Anderson (1968); a discussion of mechanisms in solid CO was given by Chrisey et al. (1990) and Philippe et al. (1997). The radiation chemical processes start with the primary excitation or ionization collisions, which are followed by a plethora of processes such as dissociation, recombination, collisions involving secondary electrons, diffusion, trapping and chemical reactions. The primary event depends on the projectile. Lyman-α photons can only produce excitations since their energy is smaller than the 12.6 eV ionization energy of solid CO (Jacobi & Rotermund 1982). Fast ions may produce closely spaced excitations or ionizations that can interact producing effects with a probability that is not linear with energy deposition. Therefore, we cannot expect a priori that photons and ions produce the same radiolytic effects. Figure 6 shows a comparison, in the 2400–1900 cm^{-1} range, between the spectrum of pure ^{13}CO as deposited and the spectra taken after UV photolysis and ion irradiation respectively. We notice that from a qualitative point of view the effects induced by both energetic processes are similar.

The absence of a significant ozone band at 1043 cm^{-1} in our experiments, compared to the abundant O_3 formation by irradiation of pure CO_2 ice with 10.2 eV photons (Grim & d'Hendecourt 1986) and 100 keV protons (Atteberry & Baragiola, unpublished), suggests that the produced radiolytic CO_2 is dispersed in the CO matrix. With the possible exception of O_2, C and C clusters, which absorb very weakly in the

infrared, other radiation products also have low concentrations compared to CO_2. This is consistent with the observation that the sputtered flux emanating from CO irradiated by 9 keV protons is composed mostly of CO, with 4% CO_2 and minor contributions of C_2, C and O (Schou & Pedrys 2001). Thus, we can approximate the fluence dependence of the concentration of CO_2 (N_2) with the following 2-component rate equation:

$$\mathrm{d}N_2/\mathrm{d}F = \sigma_{12}N_1 - \sigma_{21}N_2 \quad (1)$$

where F is the irradiation fluence (particles cm^{-2}), and where σ_{12} (σ_{21}) are the effective cross sections for converting CO to CO_2 (CO_2 to CO). The term "effective" is used with cross section since the processes involve not only an initial collision but also subsequent rearrangements and, in the case of incident ions, reactions with secondary particles, such as electrons. Some mechanisms to create CO_2 are:

$$\begin{aligned} \text{a)}\ X + \mathrm{CO} + \mathrm{CO} &\rightarrow \mathrm{CO}^* + \mathrm{CO} \rightarrow \mathrm{CO_2} + \mathrm{C} \\ &\rightarrow \mathrm{CO_2^*} + \mathrm{C} \\ \text{b)}\ X + \mathrm{CO} + \mathrm{CO} &\rightarrow \mathrm{CO}^+ + \mathrm{CO} \rightarrow \mathrm{CO_2^+} + \mathrm{C} + \mathrm{e}^- \\ &\rightarrow \mathrm{CO_2} + \mathrm{C} \end{aligned}$$

where X denotes the incident particle (photon or ion). The ionic reaction is energetically only allowed for incident protons. Production of CO from CO_2 can occur through direct dissociation or through an intermediate step involving an exciton (Abe & Onaka 1984)

$$\text{c)}\ X + \mathrm{CO_2} \rightarrow \mathrm{CO_2^*} \rightarrow \mathrm{CO} + \mathrm{O}.$$

The resulting O can associate with another O and diffuse like O_2 outside the solid (Harteck & Dondes 1955; Cornelison et al. 1998), can combine with the C left over from reaction a), or can reform CO_2 by reacting with an adjacent CO, although it has been argued that this does not occur at low temperatures due to an activation barrier (Grim & d'Hendecourt 1986; Harteck & Dondes 1955). Alternative paths for oxygen atoms are the oxidation of CO_2 into carbon trioxide (Moll et al. 1966) and the oxidation of other minor carbonaceous species. To approximate the fluence dependence of the CO concentration (N_1), we can write the following 2-component rate equation:

$$\mathrm{d}N_1/\mathrm{d}F = \sigma_{\mathrm{c}}N_2 - \sigma_{\mathrm{d}}N_1 \quad (2)$$

where $\sigma_{\mathrm{c}}(\sigma_{\mathrm{d}})$ are the effective cross sections for converting CO_2 to CO (CO to CO_2). Relations between cross sections in Eqs. (1) and (2) are obtained by evaluating the reactions occuring during irradiation. Reaction a) yields: $\sigma_{12} = 0.5\ \sigma_{\mathrm{d}}$, because it essentially takes two CO molecules to create one CO_2 molecule. Oxygen from reaction c) together with the residual C atom from reaction a), yields: $\sigma_{21} = 0.5\ \sigma_{\mathrm{c}}$. Thus, Eq. (2) can be rewritten as

$$\mathrm{d}N_1/\mathrm{d}F = 2\sigma_{21}N_2 - 2\sigma_{12}N_1. \quad (3)$$

We can replace N_1 in Eq. (1) by $N_1 = N_1^0 - 2N_2$ since the number of CO molecules decreases by two when a CO_2 molecule is formed. Therefore,

$$\mathrm{d}N_2/\mathrm{d}F = \sigma_{12}N_1^0 - (2\sigma_{12} + \sigma_{21})N_2. \quad (4)$$

The rate equations now can be readily integrated using the initial conditions at $F = 0$: $N_2^0 = 0$, $N_1 = N_1^0$, to give:

$$N_2 = N_{2\infty}\left[1 - \mathrm{e}^{-(2\sigma_{12}+\sigma_{21})F}\right] \quad (5)$$

$$N_1 = N_{1\infty}\left[1 + \left(2\frac{\sigma_{12}}{\sigma_{21}}\mathrm{e}^{-(2\sigma_{12}+\sigma_{21})F}\right)\right], \quad (6)$$

where $N_{2\infty} = N_1^0\sigma_{12}/(2\sigma_{12} + \sigma_{21})$

and $N_{1\infty} = N_1^0\sigma_{21}/(2\sigma_{12} + \sigma_{21})$.

For UV photolysis, one cannot use these expressions as a general tool for quantitative analysis, because the incident UV flux may attenuate significantly in the film. Thus, we modify the equations to include the variation of the flux with depth, x, in the film. We begin by considering the CO_2 formation in Eq. (5) as representing a differential slab with thickness dx at x, over which attenuation would be negligible:

$$\begin{aligned} N_2\mathrm{d}x &= N_{2\infty}\left[1 - \mathrm{e}^{-(2\sigma_{12}+\sigma_{21})F}\right]\mathrm{d}x \\ &= N_{2\infty}\left[1 - \mathrm{e}^{-(2\sigma_{12}+\sigma_{21})F_0\mathrm{e}^{-\alpha x}}\right]\mathrm{d}x \end{aligned} \quad (7)$$

where $F_0 = (1-r)\int\phi\,\mathrm{d}t$, r is the amount of light reflected at the surface of the film, ϕ is the incident photon flux, $\alpha = \sigma_{\mathrm{a}}N_1^0$, and σ_{a} is the absorption cross section. Integrating this over the film thickness d yields the column density of CO_2 molecules, η_2:

$$\begin{aligned} \eta_2 = \frac{\eta_{2\infty}}{\sigma_{\mathrm{a}}N_1^0 d}\Big\{&\alpha d + E_i\left[-(2\sigma_{12}+\sigma_{21})F_0\mathrm{e}^{-\alpha d}\right] \\ &-E_i\left[-(2\sigma_{12}+\sigma_{21})F_0\right]\Big\} \end{aligned} \quad (8)$$

where $E_i[z] = -\int_{-z}^{\infty}\mathrm{e}^{-t}/t\mathrm{d}t$ is the exponential integral. A least-square fit to the data, as shown in Fig. 2, yields values of $2\sigma_{12} + \sigma_{21}$ and $\eta_{2\infty}$. The agreement with the experimental results is very satisfactory considering the simplicity of the model. The differences at high fluences are most likely caused by the neglect of other components, like C_3O_2, which build up in the ice. An alternative to obtaining the values for $\eta_{2\infty}$ from the fit is to plot η_2 vs. $1/F_0$ and extrapolate to $1/F_0 \rightarrow 0$; both values are used in the calculation of σ_{12} to obtain a measure of the uncertainty in the procedure. Even more accurate values can be obtained by including only low fluence values, where the destruction of CO_2 is not yet significant and the neglect of higher order processes is more satisfactory. In this low-F limit,

$$\mathrm{d}\eta_2 = F(x)\sigma_{12}N_1\mathrm{d}x \quad (9)$$

where $F(x)$ is the incident fluence in a slab of material at x, $x + \mathrm{d}x$. Integration gives:

$$\eta_2 = \sigma_{12}N_1\int F_0\mathrm{e}^{-\alpha x}\mathrm{d}x \quad (10)$$

where $\int F_0\mathrm{e}^{-\alpha x}\mathrm{d}x = F_{\mathrm{a}}/\alpha$. Recalling that $\alpha = \sigma_{\mathrm{a}}N_1$,

$$\eta_2 = \frac{\sigma_{12}}{\sigma_{\mathrm{a}}}F_{\mathrm{a}} \quad (11)$$

where F_{a} is the number of photons absorbed cm^{-2}. By plotting η_2 vs. F_{a} for a sample of any thickness at low fluences,

Table 2. Measured and calculated values. The $\eta_{2\infty}$ values are extrapolated, see text. (The number between parenthesis indicates the error in the last significant digit.)

	200 keV H^+	Lyman-α	Lyman-α
Thickness	262 nm	262 nm	140 nm
$\eta_{2\infty}$ (CO_2 cm^{-2})	$2.7(3) \times 10^{16}$	$9.0(2) \times 10^{15}$	$5.0(4) \times 10^{15}$
% CO_2 ($100\frac{\eta_{2\infty}}{\eta_{1\infty}}$)	6.4	2.0	2.1
σ_{12} (cm^2)	$2.2(2) \times 10^{-16}$	$1.5(2) \times 10^{-19}$	$1.6(2) \times 10^{-19}$
σ_{21} (cm^2)	$3.1(2) \times 10^{-15}$	$8.3(3) \times 10^{-18}$ (*)	$8.3(3) \times 10^{-18}$ (*)
G	0.62(8)	0.57(8)	0.61(8)
σ_a (cm^2)	–	$2.6(1) \times 10^{-18}$	–

(*) Obtained from the large fluence model.

Table 3. Values derived from the fluence dependence of CO destruction in the 200 keV irradiation of a 262 nm CO film. (The number between parenthesis indicates the error in the last significant digit.)

	200 keV H^+
$\eta_{1\infty}$	$4.2(1) \times 10^{17}$ CO cm^{-2}
σ_{12}	$1.4(4) \times 10^{-16}$ cm^2
σ_{21}	$3.0(3) \times 10^{-15}$ cm^2

one can find a value for σ_{12}, which is given in Table 2. In two UV photolysis experiments with films of thickness 140 nm and 262 nm we obtain the same values for σ_{12} within error using the low fluence method and our general method. Then, we obtain σ_{21} from the general fit for $2\sigma_{12} + \sigma_{21}$ and give the value in the table as well. The value for σ_{12} is an order of magnitude higher than that calculated by Gerakines et al. (1996). A possible reason is that the authors overestimated their photon flux, as discussed by Watanabe & Kouchi (2001).

The same formalism described above can be applied to ion irradiation, taking into account that there is no significant attenuation of the flux or energy of the ions in the film. We have verified, with the TRIM code (Ziegler 2003), that the penetration depth of 200 keV protons is greater than the thickness of our CO samples (262 nm) and that the energy deposited uniformly throughout the sample. Direct application of Eqs. (5) and (6) produces values for σ_{12} and σ_{21} also given in Table 2. Here, and in the following, the number between parenthesis indicates the error in the last significant digit.

In addition to fitting the $\eta_2(F)$ curve we can also fit the destruction of CO. As mentioned above, we could detect a significant decrease in η_1 within errors only in the case of ion irradiation. The fit to $\eta_1(F)$, shown in Fig. 5, yields the values for σ_{12} and σ_{21} listed in Table 3.

We find that the values of σ_{12} and σ_{21} derived from $\eta_1(F)$ are close to those derived from $\eta_2(F)$, indicating that other molecules play minor roles in comparison to CO and CO_2, as is also evident in the infrared spectrum.

4.2. Comparison of photolysis and ion-induced radiolysis

The traditional data reduction that allows comparative study of radiation effects by different energetic particles is the radiation yield G, defined as the number of products produced by 100 eV of energy absorbed. It is clear from the fluence dependence of the column densities that G depends on F as well. Here we calculate the *initial* yield, obtained in the limit of low fluences and thin films. In the case of photolysis with 10.2 eV photons,

$$G = \frac{100}{10.2}\frac{\sigma_{12}}{\sigma_a}. \tag{12}$$

In the case of ion irradiation, we obtain ΔE, the energy deposited by the ions in the film from known values of the stopping power $S = \mathrm{d}E/\mathrm{d}\eta$, the column density of the film, η_1, and the angle of incidence θ ($\Delta E = S\,\eta_1/\cos(\theta)$).

$$G = \frac{100}{\Delta E}\sigma_{12}\eta_1 = 100\frac{\sigma_{12}}{S}\cos(\theta). \tag{13}$$

Using $S = 2.5\times10^{-14}$ eV cm^2/CO for 200 keV H^+ from the tabulation in the Stopping and Ranges module of the SRIM2003 package (Ziegler 2003), $\Delta E = 15.6$ keV for the used oblique incidence ($\theta = 45°$). The values of the radiation yield G are given in Table 4 and compared with literature values. The error in G values calculated here includes the uncertainty in S.

We notice that the G values obtained here differ from those obtained by Gerakines & Moore (2001). The higher $G(CO_2)$ value reported by Gerakines & Moore (2001) for UV photolysis could be due to the build-up of gas phase CO_2, since they used ^{12}CO to prepare their film, and also might have resulted from a different derivation of G: we considered only photons absorbed by the film, while they assumed that all photons incident on the film are absorbed (Gerakines et al. 2000). In the case of ion irradiation, it is not clear why the G values are different.

It is interesting to note that the radiation yields in solid CO are much smaller than those for the gas phase: $G(CO_2) \sim 2$ and G(-CO) between 5 and 19 (Anderson 1968). This phase difference is a commonly observed phenomenon in radiolysis and is attributed to the cage effect (Franck & Rabinowitsch 1934; Johnson et al. 1992), where dissociation products scatter with surrounding molecules in the solid (the cage) giving a high probability of recombination.

As a complement to the calculation of G, one can also qualitatively compare the two experiments by using a common radiation dose parameter, the average energy absorbed per molecule. A unit useful to compare with measurements on

Table 4. Initial radiation yields G, in molecules/100 eV, for CO_2 production and CO destruction. The CO destruction yield, G(-CO) is calculated with $2\sigma_{12}$ (see text; the number between parenthesis indicates the error in the last significant digit).

Excitation	Energy	$G(CO_2)$	G(-CO)	Reference
Ly-α	10.2 eV	0.9(2)		Gerakines & Moore (2001)
Ly-α	10.2 eV	0.59(8)		This work
H^+	800 keV	0.25(4)		Gerakines & Moore (2001)
H^+	200 keV	0.62(8)	0.79(9)	This work

Table 5. Observed column densities of CO(apolar) and CO_2 in interstellar ices and an estimation of the amount of CO_2 formed after processing of CO-rich icy mantles.

Source	Observed values (mol cm^{-2})		Estimated CO_2 (mol cm^{-2})	
	η_{CO}(apolar)	η_{CO_2}	1 MeV H^+	Lyman-α
Elias 16	5.6×10^{17} (a)	4.6×10^{17} (b)	2.6×10^{16}	1.1×10^{16}
R CrA IRS1	4.1×10^{17} (c)	6.2×10^{17} (b)	1.9×10^{16}	8.2×10^{15}
NGC 7538 IRS9	11×10^{17} (c)	16×10^{17} (b)	5.2×10^{16}	2.2×10^{16}

(a) Chiar et al. (1995); (b) Gerakines et al. (1999); (c) Chiar et al. (1998).

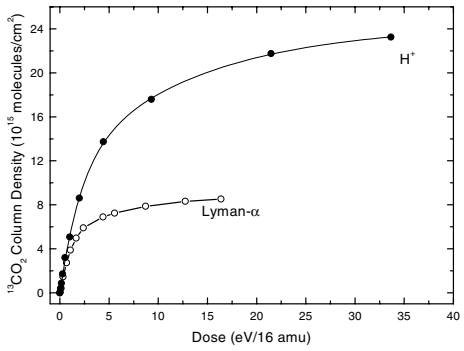

Fig. 7. Comparison of the column density of $^{13}CO_2$ formed from 262 nm ^{13}CO ice film at 16 K by irradiation with 10.2 eV photons and 200 keV protons.

other condensed gases was proposed by Strazzulla & Johnson (1991), obtained by dividing the energy absorbed by 16 amu, the mass of a typical molecule (e.g. CH_4). The comparison using this unit is shown in Fig. 7. It is interesting to note that while the initial production rate of CO_2 per unit energy deposited is similar for 10.2 eV photons and 200 keV protons, the equilibrium CO_2 concentration is three times higher for ion irradiation. This is due to the different ratios between the formation and destruction cross sections for ion irradiation and UV photolysis.

4.3. Solid CO in the interstellar medium

Infrared observations have shown that solid CO is present in icy grain mantles in quiescent interstellar clouds and in both low-mass and high-mass star forming regions. Its abundance ranges from 0% to 50% with respect to water ice (e.g., Tielens et al. 1991; Chiar et al. 1994, 1995, 1998; Teixeira et al. 1998; Pontoppidan et al. 2003). A detailed study of the profile of the solid ^{12}CO feature at 4.67 μm (2140 cm^{-1}) has shown that it can be divided into two separate components. On the basis of detailed comparisons with laboratory spectra these two components have been named polar and apolar indicating that at least two molecular environments exist in icy grain mantles. In particular, the polar component is attributed to CO mixed in with water ice (e.g. Tielens et al. 1991; Kerr et al. 1993; Chiar et al. 1994, 1995, 1998) or formed after cosmic ray irradiation of icy mixtures containing carbon-bearing species (Palumbo & Strazzulla 1993; Teixeira et al. 1998), while the apolar component is attributed to ice mantles of pure CO or CO mixed with apolar species such as O_2, N_2, and CO_2. Recent, high resolution, high S/N ratio observations of a large sample of low-mass star forming clouds indicate that the observed band profile of solid CO can be decomposed into three components suggesting that three distinct molecular environments of solid CO exist in the interstellar medium (Pontoppidan et al. 2003). In dense clouds, icy mantles are processed by cosmic rays, UV photolysis and thermal annealing. It has been suggested that carbon dioxide observed in interstellar ices could be formed after cosmic ray irradiation and/or UV photolysis of icy mantles. On the basis of the experimental results reported above, we have estimated the amount of interstellar CO_2 formed from processing of CO-rich icy mantles (i.e. the apolar component). Following Mennella et al. (2003), we consider the approximation of monoenergetic 1 MeV protons and assume that in dense interstellar regions the 1 MeV proton flux ($\Phi_{p,1\ \mathrm{MeV}}$) is equal to 1 proton cm^{-2} s^{-1} and that the internal UV flux, due to cosmic-ray induced fluorescence of molecular hydrogen, (Φ_{UV}) is equal to 4.8×10^3 photons cm^{-2} s^{-1}. Using the observed column density of apolar CO, Eq. (5), and the parameter values reported in Table 2, we have calculated the amount of expected solid CO_2 towards three different lines of sight (Table 5) namely Elias 16 (a field star), R CrA IRS1 (a low mass protostar) and NGC 7538 IRS9 (a high mass protostar). In the calculatation we have assumed a typical cloud lifetime of 3×10^7 y.

Our experimental results on the production of carbon dioxide after ion irradiation are based on experiments performed using 200 keV H^+ ions. We have obtained the formation and

destruction cross sections by 1 MeV protons from those obtained in our irradiation experiments with 200 keV protons assuming they scale with the stopping power (S). For H^+ ions impinging on pure CO ice the ratio S(200 keV)/S(1 MeV) is 2.5.

We find (Table 5) that an amount between 1% to 6% of the observed interstellar solid CO_2 can be formed after processing CO-rich icy mantles, indicating that this mechanism is not dominant in forming interstellar CO_2. This result seems to be in agreement with the results obtained after fitting the profile of the observed CO_2 features with laboratory spectra. As shown by Gerakines et al. (1999), laboratory spectra of CO_2 mixed with apolar species (such as CO) do not provide a good fit of the observed features. However, this result does not exclude that solid CO_2 is formed after cosmic-ray irradiation and/or UV photolysis of interstellar ices different to pure CO. Formation cross section values strongly depend on the ice considered. For example, Watanabe & Kouchi (2002) have reported a rate of 2.5×10^{-4} s^{-1} for the formation of CO_2 in a H_2O:CO = 10:1 mixture at 12 K after UV photolysis from which a formation cross section equal to 1.4×10^{-18} cm^2 was derived (Mennella et al. 2004). Mennella et al. (2004) report a value of 2.4×10^{-15} cm^2 for the formation cross section of CO_2 after ion irradiation of a H_2O:CO = 10:1 ice mixture. Both values are about an order of magnitude greater than the respective cross sections reported in Table 2, indicating that, given the same amount of energy released to the icy sample, a greater amount of CO_2 is formed in H_2O-rich mixtures.

5. Conclusions

The use of isotope labelling has allowed us to obtain data that is free from contamination from residual carbon dioxide in a vacuum system which would otherwise produce an overestimate of the radiation yields. To quantify our results, we developed a simple two-component model that accounts for the attenuation of Lyman-α radiation as it passes through the ice. The model adequately describes the behaviour of CO_2 production at low fluences as well as the destruction of CO. The initial production rate of CO_2 per unit energy deposited is similar for 10.2 eV photons and 200 keV protons, but the equilibrium CO_2 concentration is three times larger for ion irradiation.

Acknowledgements. M.J.L. was supported by the Alcoa International Graduate Research Fellowship. We are grateful to F. Spinella for his valuable assistance in the laboratory. This work has been financially supported by the Italian Ministero dell'Istruzione, dell'Università e della Ricerca (MIUR).

References

Abe, H., & Onaka. R. 1984, J. Phys. Soc. Jpn, 53, 1176
Anderson, A. R. 1968, Inorganic Gases, Ch. 5 in Fundamental Processes in Radiation Chemistry, ed. P. Ausloos (NY: Wiley)
Baragiola, R. A., Vidal, R. A., Svendsen, W., et al. 2003, Nucl. Instr. Methods. Phys. Res. B, 209, 294
Baratta, G. A., & Palumbo, M. E. 1998, JOSA A, 15, 3076
Baratta, G. A., Leto, G., & Palumbo, M. E. 2002, A&A, 384, 343
Brown, W. L., Augustyniak, W. M., Macartonio, K. J., et al. 1984, Nucl. Instr. Meth. Phys. Res. B, 1, 307
Chiar, J. E., Adamson A. J., & Whittet, D. C. B. 1994, ApJ, 426, 240
Chiar, J. E., Adamson A. J., & Whittet, D. C. B. 1995, ApJ, 455, 234
Chiar, J. E., Gerakines, P. A., Whittet, D. C. B., et al. 1998, ApJ, 498, 716
Chrisey, D. B., Brown, W. L., & Boring, J. W. 1990, Surf. Sci., 225, 130
Cornelison, D. M., Dillingham, T. R., Tegler, S. C., et al. 1998, ApJ, 505, 443
Cottin, H., Moore, M. H., & Bénilan, Y. 2003, ApJ, 590, 874
de Graauw, Th., Whitthet, D. C. B., Gerakines, P. A., et al. 1996, A&A, 315, L345
d'Hendecourt, L. B., & Jourdain de Muizon, M. 1989, A&A, 223, L5
Franck, J., & Rabinowitsch, E. 1934, Trans. Farad. Soc., 30, 120
Gerakines, P. A., & Moore, M. H. 2001, Icarus, 154, 372
Gerakines, P. A., Moore, M. H., & Hudson, R. L. 2000, A&A, 357, 793
Gerakines, P. A., Schutte, W. A., & Ehrenfreund, P. 1996, A&A, 312, 289
Gerakines, P. A., Whittet, D. C. B., Ehrenfreund, P., et al. 1999, ApJ, 522, 357
Grim, R. J. A., & d'Hendecourt, L. B. 1986, A&A, 167, 161
Harteck, P., & Dondes, S. 1955, J. Chem. Phys., 23, 902
Jacobi, K., & Rotermund, H. H. 1982, Surf. Sci., 116, 435
Jiang, G. J., Person, W. B., & Brown, K. G. 1975, J. Chem. Phys., 64, 1201
Johnson, R. E., Liu, M., Baragiola, R. A., & Boring, J. W. 1992, Energy Transfer Processes and Retention of Hot Atoms, in Handbook of Hot Atom Chemistry, ed. J.-P. Adloff et al. (Tokyo: Kodansha), 156
Kerr, T. H., Adamson, A. J., & Whittet, D. C. B. 1993, MNRAS, 262, 1047
Leto, G., & Baratta, G. A. 2003, A&A, 397, 7
Mathis, J. S., Mezger, P. G., & Panagia, N. 1983, A&A, 128, 212
Mennella, V., Baratta, G. A., Esposito, A., Ferini, G., & Pendleton, Y. J. 2003, ApJ, 587, 727
Mennella, V., Palumbo, M. E., & Baratta, G. A. 2004, ApJ, 615, 1073
Moll, N. G., Clutter, D. R., & Thompson, W. E. 1966, J. Chem. Phys., 45, 4469
Palumbo, M. E., & Strazzulla, G. 1993, A&A, 269, 568
Philippe, L., Hirayama, T., Ramage, M. J., et al. 1997, J. Chem. Phys., 106, 7072
Pontoppidan, K. M., Fraser, H. J., Dartois, E., et al. 2003, A&A, 408, 981
Roser, J. E., Vidali, G., Manicò, G., & Pirronello, V. 2001, ApJ, 555, L61
Roux, J. A., Wood, B. E., Smith, A. M., & Plyler, R. R. 1980, AEDC-TR-79-81
Schou, J., & Pedrys, R. 2001, JGR E, 106, 33, 309
Strazzulla, G., & Johnson, R. E. 1991, in Comets in the Post Halley Era, ed. R. L. Newburn, M. Neugebauer, & J. H. Rahe (Dordrecht: Kluwer), 243
Strazzulla, G., Brucato, J. R., Palumbo, M. E., & Satorre, M. A. 1997, A&A, 321, 618
Teixeira, T. C., Emerson, J. P., & Palumbo, M. E. 1998, A&A, 330, 711
Tielens, A. G. G. M., Tokunaga, A. T., Geballe, T. R., & Baas, F. 1991, ApJ, 381, 181
Trottier, A., & Brooks, R. L. 2004, ApJ, 612, 1214
Watanabe, N., & Kouchi, A. 2001, ApJ, 567, 651
Westley, M. S., Baragiola, R. A., Johnson, R. E., & Baratta, G. A. 1995a, Nature, 373, 405
Westley, M. S., Baragiola, R. A., Johnson, R. E., & Baratta, G. A. 1995b, Planet. Space Sci., 43, 1311
Westley, M. S., Baratta, G. A., & Baragiola, R. A. 1998, J. Chem. Phys., 108, 3321
Yamada, H., & Person, W. B. 1964, J. Chem. Phys., 41, 2478
Ziegler, J. F. 2003, Stopping and Range of Ions in Matter SRIM2003 (available at `www.srim.org`)